JOURNAL OF APPLIED ELECTROCHEMISTRY 8 (1978) 49–59

Non-linear electric analogues of the current distribution in porous electrodes

K.-J. EULER

Arbeitsgurppe Technische Physik der Gesamthochschule Kassel, AVZ, OE 03, Heinrich-Plett-Straße 40 D 3500 Kassel, West Germany

B. SEIM

Eichenweg 12, D 2070 Ahrensburg, West Germany

Received 9 May 1977

Porous battery electrodes can, with respect to their volumetric current distribution, be regarded as electrical networks. Linear, time-independent networks again can be treated by analytical methods. In some practical cases, however, deviations have to be considered: non-linear overvoltage functions, changing conductivities. Current distribution in such non-linear and time-dependent systems can be evaluated either by numerical computor calculations, or by the application of corresponding electrical analogues. The latter way is fairly simple and will be treated here.

The observed overvoltage functions can be generated by semiconducting diodes. Changing conductivities have been generated by adjustable resistors. Application of special automatic devices, e.g. diaphragms with closing pores, seems possible but has not been effected so far. Voltage and current scales have to be adapted to the characteristics of the electronic components.

In general, we can state, that in some practical electrodes the real overvoltage functions may change the current distribution markedly. Particular 'shoulders' in the distribution curves are observed, which ameliorate the electrode utilization. Introduction of measured ionic conductivity changes certainly influences the current distribution but results in deteriorations of the predicted electrode characteristics.

Poröse Batterie-Elektroden können bezüglich ihrer volumetrischen Stromverteilung als elektrische Netzwerke angesehen werden. Lineare, von der Zeit unabhängige Netzwerke hinwiederum können mit analytischen Verfahren theoretisch behandelt werden. In einigen technischen Fällen müssen aber Abweichungen davon berücksichtigt werden: nichtlineare Überspannungs-Funktionen, zeitabhängige Leitfähigkeit. Die Stromverteilung in solchen nichtlinearen und zeitabhängigen Systemen kann entweder numerisch mit einem Rechner oder durch die Untersuchung entsprechender elektrischen Analogmodelle ermittelt werden. Der letztere Weg ist verhältnismässig einfach und wird hier behandelt.

Gemessene Überspannungs-Funktionen können z.B. durch Halbleiter-Dioden nachgebildet werden. Änderungen der Leitfähigkeit sind durch nachgeregelte Widerstände berücksichtigt worden. Dazu automatische Bauelemente zu verwenden, z.B. Diaphragmen mit Poren, die sich schliessen, erscheint möglich, ist aber noch nicht erfolgreich durchgeführt worden. Die Maßstäbe für Spannung und Stromstärke müssen den Eigenschaften der verwendeten elektronischen Bauelemente angepaßt werden.

Als allgemeingültiges Ergebnis kann man festhalten, dass in technischen Elektroden die tatsächlichen Überspannungs-Funktionen die Stromverteilung merklich beeinflussen können. Absätze oder 'Schultern' in den Verteilungs-Funktionen werden beobachtet, welche die Elektroden-Ausnutzung verbessern. Auch die Berücksichtigung der Änderungen des Ionen-Widerstandes hat Einfluss auf die Stromverteilung, führt aber zu einer Verschlechterung der vorherzusagenden Elektroden-Eigenschaften.

1. Introduction

In the following paper the spatial distribution of the *volumetric* current density (A cm^{-3}) over the depth of porous battery electrodes will be considered. Schoop [2] noted in 1898 disproportionate spatial distributions of lead dioxide in battery plates. In 1925, Fischbeck and Einecke [3–6] observed irregular colour changes in reduced powder electrodes. Both authors were not able to interpret their results correctly. The interplay between electronic and ionic conduction in porous electrodes was recognized by Russian authors [7] first in 1948. A few years earlier, Coleman [8–10] investigated the current distribution in positive electrodes of dry cells. The complete electric statement of the problem was put forward in 1958 by Euler [11–13].

2. Porous electrode as an electrical network

Fig. 1 shows the complete d.c. network to be investigated. Electrons migrate perpendicularly to the electrode surface through a chain of resistors R_e; ions migrate through the chain of resistors R_i. Neither R_e nor R_i depend on the electric current. In semi-infinite plain electrodes R_e and R_i are independent of the depth coordinate z. This is the simplest geometry. However, circular or irregular electrodes can be treated also, including the case of electrodes having current components perpendicular to z. The inner surface of the porous electrode forms the boundary between electronic and ionic conductors and the potential here is U. As long as the potential does not depend on the coordinate z, it can be neglected. The overvoltage (polarization) $\eta\,(i)$ is a rather complicated function of the *real* current density. In general, we can use the functions given in Table 1. To describe the electrodes, we need only two parameters, R_e and R_i, and the overvoltage function $\eta(i)$, the latter represented possibly by a third resistance R_η. The first aim of our investigation was, to approximate $\eta(i)$ by electronic components, e.g. by semiconducting diodes, and to look at the consequences.

Table 1. General types of overvoltage functions to be expected in practical battery electrodes

(i) complete, e.g. measured functions $\eta = f(i)$
(ii) exponential redox type
$i = i_0 \{A \exp(a\eta) - B \exp(-b\eta)\}$
i_0 = exchange current
A, a constants of the forward reaction
B, b constans of the back reaction
(iii) logarithmic Tafel type
$\eta = \frac{1}{a} \ln (i/i_0 A)$
(iv) polynomic (or linear)
$\eta = R_\eta i + r_1 i^2 + r_2 i^3 \ldots$

These four types can be observed combined with limiting currents.

3. Changes during discharge and charge

To describe the electrodes during charge or discharge, not only the initial parameters R_e, R_i and η have to be considered, but also their variation with time. It seems hardly possible, to

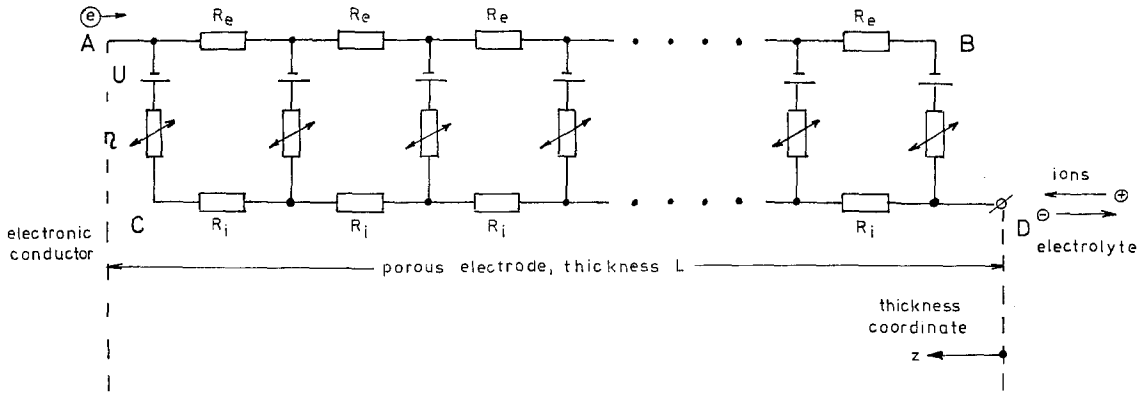

Fig. 1. Electrical network substituting a flat porous battery electrode. Arrows indicate discharge of a positive electrode. A, B, C, and D: electrical corners. L, Thickness divided in slices Δz; A, geometrical area; $R_e = \rho_e z/A$; $R_i = \rho_i z/A$; ρ_e, electronic resistivity; ρ_i, ionic resistivity; U, electrode potential; η, overvoltage related to the slice volume $A\Delta z$.

measure and separate these parameters without destroying the cells. However, we can state that

(i) R_e and R_i can be followed together by means of a.c. methods. Since R_e remains nearly constant, measured changes can be ascribed to R_i.

(ii) In our 18 years of experience changes of $\eta(i)$ do not influence the current distribution too much.

Thus, we have to consider only changing, particularly rising, R_i. It has been measured at electrodes of various thicknesses, extrapolated to zero thickness and introduced by adjustment of the R_i representing the network mesh in question, either by manual action, or by calculation.

Depending on phase width, concentration changes etc., fairly large potential profiles can arise [14]. The influence of R_i has been investigated in linear electrode models [15, 16]; its influence in the correlation to non-linear networks will be treated next [17].

4. Electric generation of overvoltage functions

If the general behaviour of a certain class of battery electrodes is known, the linear overvoltage approximation can be used:

$$R_\eta \approx \eta/i\Delta z. \quad \Delta z \text{ thickness element.}$$

Overvoltage functions $\eta(i)$ are measured using electrodes of different thicknesses L_1, L_2, L_3, etc., and have to be extrapolated to $L \to 0$. A mean value $\bar{i}$, given in mA cm^{-3} has to be inserted. Supposing the electrode potential U does *not* depend on z, the problem can be solved exactly, for flat electrodes [18] as well as for cylindrical ones [19]. The 'linear' procedure is well suited for the investigation of small material changes, porosity changes, additives, size changes, etc.

However, large changes, changed manufacturing processes, uncommon charge/discharge conditions, freezing electrolyte, etc., will introduce insupportable uncertainties. Under such circumstances, or if uncommon electrode types are to be investigated, a better overvoltage approximation becomes necessary. Stein [20, 21], Newman and Tobias [22], Grens II [23], Fleck, Hanson and Tobias [24], and Alkire [25], introduced computational methods. The authors investigated electrode models taking into consideration pore size and distribution, concentration changes, diffusion, ion transfer, etc. Reducing a current distribution problem to its true origin in electrochemistry, anyway is very meritorious. However, as has been shown earlier [26], it is hardly possible to measure or calculate the necessary parameters. Therefore, a more pragmatic treatment seems adequate for practical problems, even accepting sweeping simplifications.

Instead of porous electrode models, electric circuits and networks are substituted, which can be understood very easily, see Fig. 1. The computational or experimental treatment is quite simple. Therefore, this method seems preferable in most practical cases, in as much, as changing parameters, inhomogeneous electrode potentials, etc., can be introduced in these electrical analogues also.

In Table 2 different overvoltage characteristics are compiled. As a principal result, we have to state, that in practical problems only two of the expected overvoltages types indicated in Table 1. really did occur. The battery electrodes investi-

Table 2. Overvoltage characteristics of battery electrodes under normal conditions, e.g. 20° C, normal load, not exhausted, not poisoned, but extrapolated to the thickness $L \to 0$. pct. relates to weight.

(i) $Pb/PbSO_4$ and $PbO_2/PbSO_4$ electrodes in sulphuric acid, both fully charged and 50 pct. discharged, anodic and cathodic direction, between 0 and 1000 500 mA cm^{-3} functions between linear and logarithmic.

(ii) 80 pct. NiOOH and 20 pct. graphite (pocket plates) in KOH solution both fully charged and 5 h rate discharged, cathodic direction between 0 and 1000 mA cm^{-3} purely linear overvoltage functions, see Fig. 2.

(iii) 80 pct. electrolytic manganese dioxide, 10 pct. NH_4Cl and 10 pct. carbon black, in free electrolyte consisting of 20 pct. NH_4Cl, 10 pct. $ZnCl_2$ and 70 pct. water, not discharged, cathodic direction, below 1 mA cm^{-3} linear, between 3 and 1000 mA cm^{-3} logarithmic overvoltage functions, see Figs. 3 and 4.

(iv) 80pct. electrolytic manganese dioxide and 20 pct. graphite in KOH solution, not discharged, cathodic direction, between 0 and 1000 mA cm^{-3} functions between linear and logarithmic.

(v) 90pct. HgO and 10 pct. graphite in KOH solution, not and partly discharged, cathodic direction, between 0 and 500 mA cm^{-3} functions between linear and logarithmic.

(vi) Zinc powder pellets, pure and with 10 pct. mercury, in KOH solution, not passivated, not discharged, anodic dissolution between 0 and 200 mA cm^{-3} functions between linear and logarithmic, see Fig. 5.

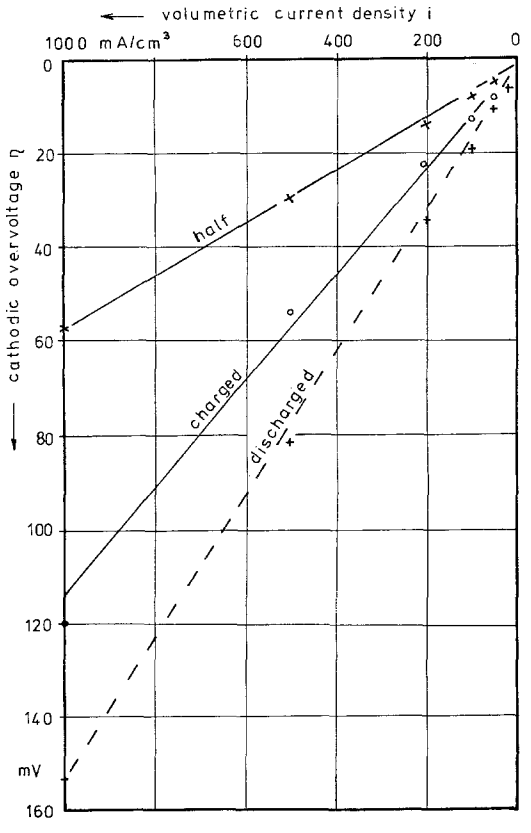

Fig. 2. Cathodic overvoltage of a 80pct. NiOOH/Ni(OH)$_2$ and 20 pct. graphite electrode as used in pocket plates, 20° C, extrapolated to thickness $L \to 0$, fully charged, half discharged and fully discharged, 5 h rate. Linear current density scale.

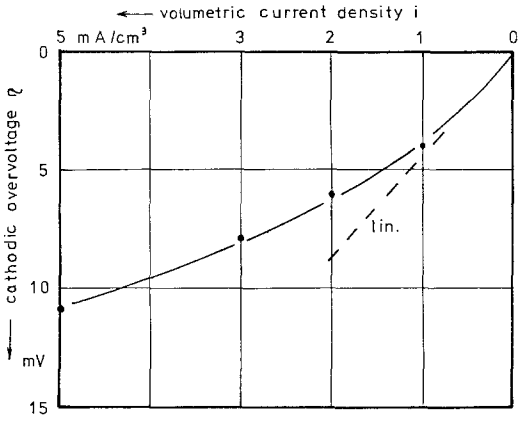

Fig. 3. Cathodic overvoltage of electrolytic manganese dioxide, 80 pct. thereof mixed with 10 pct. NH_4Cl and 10 pct. carbon black in free electrolyte consisting of 70 pct. water, 20 pct. NH_4Cl and 10 pct. $ZnCl_2$. Temperature 20° C, extrapolated to thickness $L \to 0$, not discharged. Logarithmic current density scale.

gated in our laboratory so far, have belonged to the following types:

(i) linear type $\eta \sim i$ see Fig. 2.

(ii) logarithmic type $\eta \sim \log (i/i_0)$ see Figs. 3 and 4.

(iii) intermediate type see Figs. 5 and 6.

We cannot rule out other types of overvoltage functions playing a role in other, less common electrodes, or under deviating conditions. Such circumstances may be expected in heavily com-

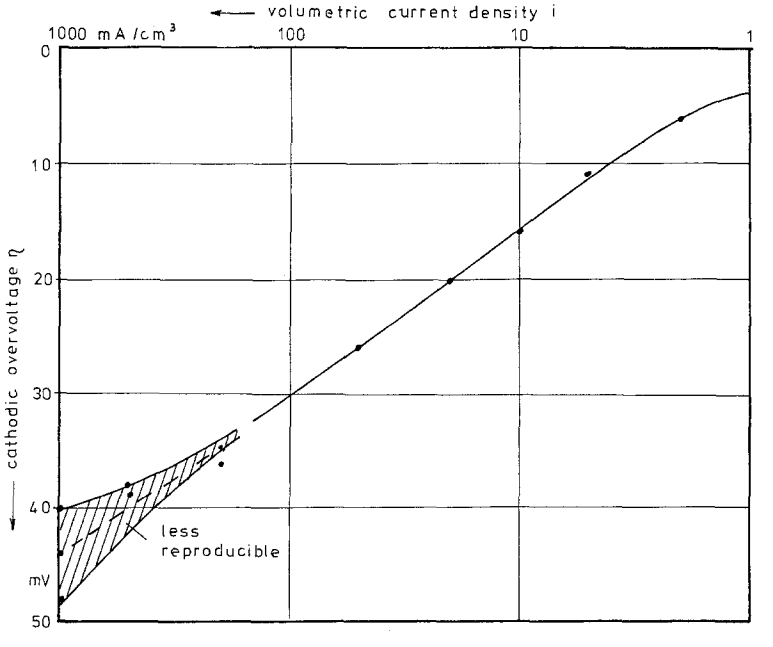

Fig. 4. Cathodic overvoltage of electrolytic manganese dioxide, similar to Fig. 3, but linear current density scale.

pressed powder electrodes, poisoned lead plates, deeply discharged electrodes, under heavy overcharge conditions with high gassing etc. These must be excluded here, because we have not investigated them so far. Also singularities can cause uncommon overvoltage behaviour.

The extrapolation to the thickness $L \to 0$ excludes automatically the diffusion resistance. Electrolyte access to the 'deeper' electrode slices in these analogues proceeds faster than in real electrodes. However, in most practical cases only the 'inner' electrolyte inside the pores is available. Its depletion changes the overvoltage as well as the electrode potential [14, 17]. The inclusion of interlayer-diffusion into electric analogues has already been tried. However, such ameliorations remain small compared with the measuring errors of the main parameters. Therefore, we exclude interlayer diffusion here.

As can be expected by the identical mathematical formalisms, logarithmic overvoltage functions can be imitated by semiconducting diodes in the forward direction. If necessary, these characteristics can be modified by series or shunt resistors, see Fig. 6. As an example, the anodic overvoltage function of pure zinc, given in Fig. 5, can be approximated by the diode OA 20 shunted by a resistor of 1000 Ohm. The best fit can be found easily using a pocket calculator or simply by graphical comparison of curves in a double logarithmic diagram. The result is compiled in Table 3. The anodic load of 100 mA cm^{-3} at the pure zinc electrode corresponds to the current of 0·088 mA at the diode resistor combination, thus giving a degression factor (volume) of $1:1136 = 8{\cdot}8 \cdot 10^{-4}\,cm^3$. In spite of this, the overvoltage 1 mV corresponds to 4·00 mV at the diode, giving a factor of 4·00. It should be possible to find even a better fit.

As well as semiconducting diodes, a fairly large number of electronic components can be used to imitate overvoltage functions. Fig. 7 surveys the different types we took into consideration. For comparison, ohmic resistors are included. *A priori*, gas-filled and vacuum tubes were excluded, because the need of filament heating renders handling rather difficult.

Barretters, i.e. iron wires in hydrogen gas atmospheres, can be used to introduce limiting currents. The main disadvantage is the high dissipated heat loss, and the slow response. The inverse behaviour, constant voltage at variable current, is exhibited by Zener diodes in the blocking direction. Negative temperature coefficient resistors (NTC) exhibit exponential characteristics $U = CI^{\beta}$. Even steeper exponents were possible by bridging the NTC resistor by an incandescent lamp (24 V/3 W). Also positive temperature coefficient resistors

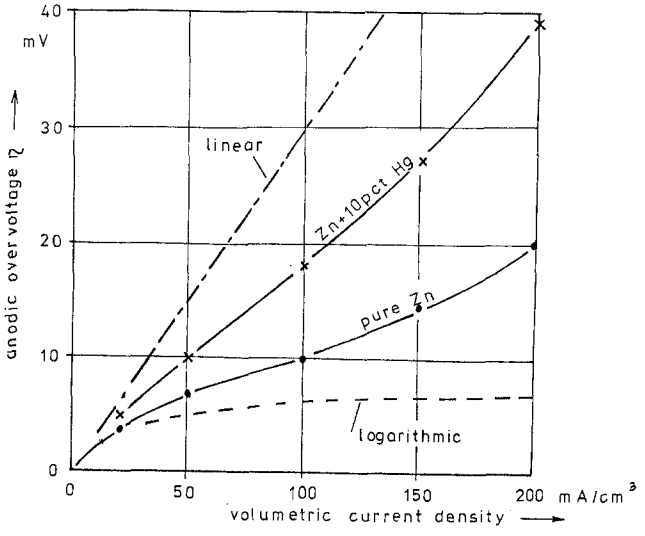

Fig. 5. Anodic overvoltage of a Zn powder electrode in KOH electrolyte, 20° C, not passivated, extrapolated to thickness $L \to 0$. Linear current density scale. For comparison, linear and logarithmic overvoltage functions are indicated.

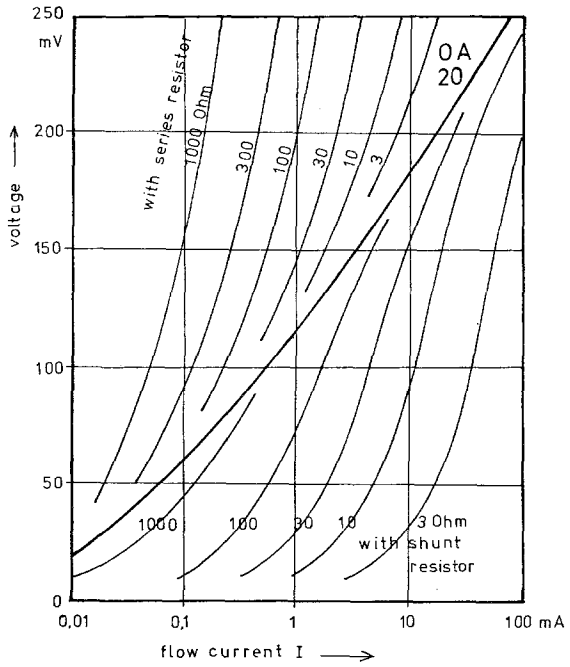

Fig. 6. Characteristics of a gold bonded Ge diode, flow direction, OA 20, alone and with series and with shunt resistors. Current scale logarithmic.

(PTC) and voltage dependent resistors (VDR) were included in Fig. 7. Bearing in mind, that mutual combinations as well as combinations with ohmic resistors are possible, one is led to the conclusion that nearly every overvoltage function can be imitated by suitable electronic components.

5. Iterative procedures

In general, non-linear components in electric analogues can be replaced by adjustable resistors, e.g. helical potentiometers, etc. The measured overvoltage function $\eta(i)$ is converted first into the replacing resistor $R(i) = \eta/i$. One starts with equal resistors $\bar{R}$ in every network mesh. $\bar{R}$ is valid for the mean current density $\bar{i} = I/V$, where I is the entire electrode current and V its volume. The measured first approximation of the current distribution $i_1(z)$ leads to a first readjustment of the resistors, resulting in a second approximation $i_2(z)$. The procedure can be repeated and converges. Depending upon the experience of the assistant and the special electrode parameters, up to six iterations are necessary to reach stationary distribution curves. It should be mentioned, that the iteration sometimes failed, if we tried to investigate singularities or striated electrodes.

In a similar way, the electrical network can be replaced by a computor programme to solve the set of Kirchhoff's mesh and knot equations. Again the first step is the insertion of constant overvoltage resistors $\bar{R}$. It is followed by a re-adjustment and a few iterations. We used both methods as well as non-linear diode networks. In our opinion, the latter deliver the desired results very quickly and with a minimum of expense. On the other hand, the electronic components have to be matched very carefully. Nevertheless, the computer results are more exact. However, as has been shown earlier [26], the accuracy is not limited by the method used, but by the uncertainties of the parameters.

6. A large MnO_2 electrode as an example

Non-linear networks were used to investigate several uncommon electrode compositions and uncommon dimensions. As a principal result, we

Table 3. Approximation of the anodic overvoltage function of pure zinc, see Fig. 5, by a semiconducting diode, OA 20, see Fig. 5, shunted by a resistor of 1000 Ohm. Current degression factor 1 : 1136 = 8·803 · 10^{-4}, voltage surmount factor r = 4·00.

Pure zinc, see Fig. 5			*Replacing diode, see Fig. 6, shunted by 1000 [Ohm]*		*Difference*
Anodic load [mA cm^{-3}]	*Overvoltage* η [mV] *measured* η	*Surmounted* ηr	*Corresponding current* [mA]	*Voltage* U_d [mV]	$U_d - \eta r$ [mV]
1·14	0·22	0·88	0·001	1	+ 0·12
3·41	0·68	2·7	0·003	3	+ 0·3
11·4	2·3	9·2	0·01	10	+ 0·8
34·1	6·3	25	0·03	25	± 0
113	12·0	48	0·1	50	+ 2
341	22	88	0·3	86	− 2

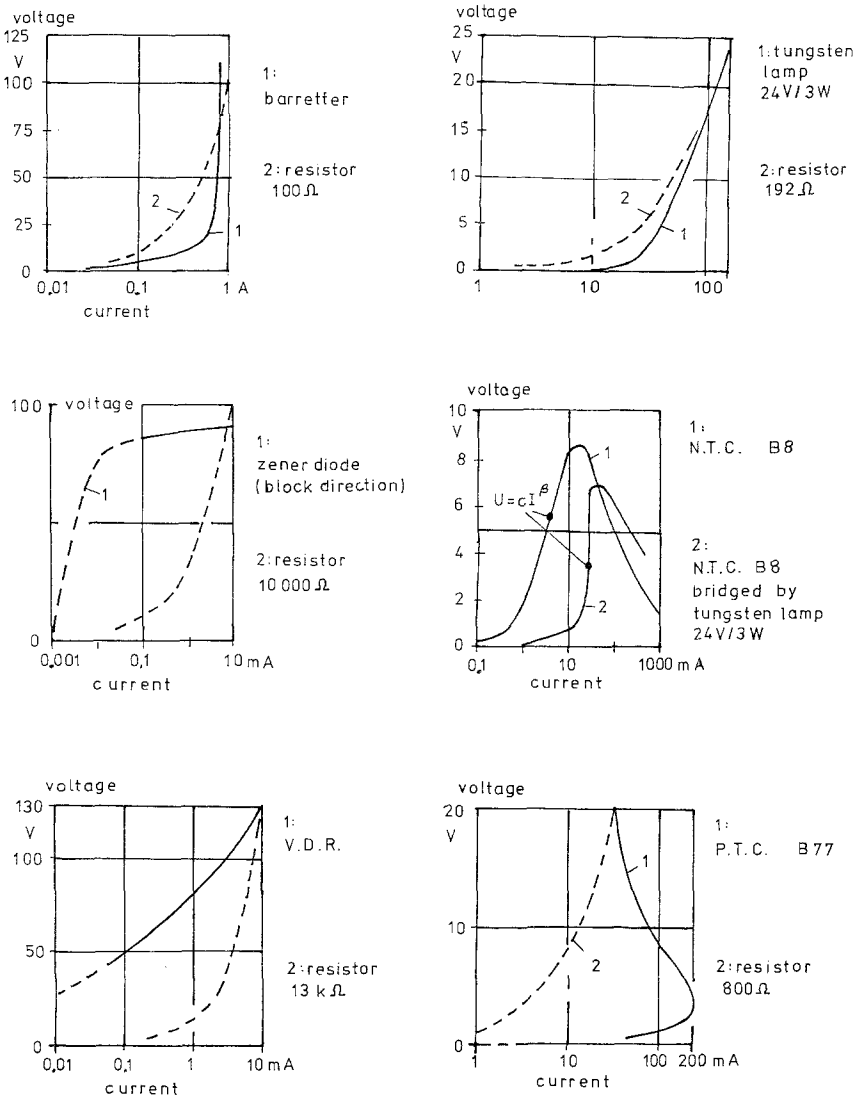

Fig. 7. Current/voltage characteristics of various electronic components.

found, that changing the active substances of porous battery electrodes does not greatly affect the general pattern of the current distribution. Always the two borders, directed to the electrolyte and to the electronic terminal have to bear the largest fractional current, the inner parts remaining nearly untouched. There is a close relation between overvoltage and useful electrode thickness: the smaller the overvoltage the more active is the electrode mass and the thinner the electrodes have to be. Inactive masses, exhibiting large overvoltage enable the use of thick electrodes. This was proven not only with the common electrode materials indicated in Table 2, but also using several others. As examples, we mention the insoluble compounds silver pyridinium perchlorate $Ag(C_5H_5N)_2ClO_4$ and barium manganate (VI) $BaMnO_4$. Current distributions, in both cases, are quite similar to the habitual curves of black mix electrodes in dry batteries, and show no advantage.

A more interesting, because deviating, result was obtained with electrodes having uncommon dimensions. For special applications (buoys), the design of large dry batteries is necessary, and this allows us to investigate electrodes of more than 150 mm working thickness. The mean flash load

applied was set to more than 10 mA cm^{-3}, which seemed not exceedingly high compared with the overvoltage curves, see e.g. Fig. 4. To solve the problem, we measured the necessary data and converted it into the electric elements, see Table 4. The current degression factor $c = 0{\cdot}010\ cm^3$ indicates, that a volumetric conversion current density i mA cm^{-3} corresponds to a diode current $I_d = ci$. Because I is measured in mA, the degression factor c has the dimension of a volume, cm^3. The voltage surmount factor r again means, that a diode voltage U_d corresponds to a lower overvoltage, $U_d = r\eta$. Both scale factors can be compensated by enlarging the longitudinal resistors by the factor $w = r/c$. In the simplest case, each network mesh represents a thickness element $\Delta z = 1$ cm and an area element $\Delta A = 1\ cm^2$, thus a volume element $\Delta\tau = 1\ cm^3$. The longitudinal electronic resistors then are $R_e = \rho_e r \Delta z / c \Delta A$ or, inserting the above given values, $R_e = 3000$ Ohm. Because both resistivities are numerically equal, the ionic longitudinal resistors also become $R_i = 3000$ Ohm.

The formal results are given in Fig. 8. The dotted lines, 'c' indicate the result of the conventional, linearized calculation. Introducing the non-linear elements makes the 'shoulders' 20 to 30 mm below the electrode's borders visible. Although the electrode behaves 'better' than predicted by the linear approximation a very large part, more than two thirds, does not work at all. We tried to ameliorate the current distribution by enlarging the electronic conductivity. This is a very old measure of the battery scientist, simply adding better electronic conductors, e.g. graphite to the black mix. The optimum result we obtained is given in Fig. 9. This is a better but not satisfactory result. The battery design therefore has been changed, replacing the large single cell – outer dimensions 400 x 400 x 400 mm^3 – by a battery of 32 air depolarized cells IEC–AS 8 connected in parallel. However, we obtained a very interesting insight into the electric processes in thick porous electrodes. As the most interesting feature, we discovered the 'shoulders' not observed so far.

Another quite simple result is the estimate of the possible short circuit (flash) current I_k. In the electric analogue, see Fig. 1, between the corner A

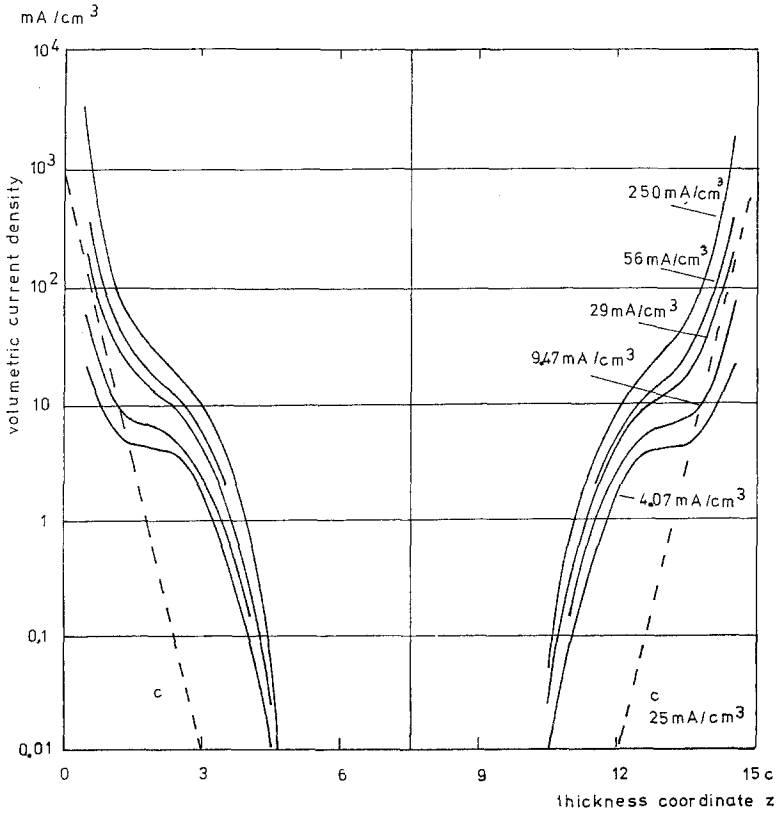

Fig. 8. Current distribution taken from a non-linear chain network representing a thick MnO_2 electrode, parameters see Table 4. The exponential lines cc correspond to a linear approximation for a mean load of 25 mA cm^{-3}.

and B or C and D, respectively, an integral resistance or an integral voltage drop U can be measured. It allows the estimate of the flash current: under flash conditions, the entire voltage reduced by the surmount factor r is equal to the rest potential U_0 of the cell. Therefore we can look at the entire current I obeying this condition. It corresponds to the flash current I_k in the same manner as every current in the analogue, namely by the application of the current degression factor c. To fulfil the flash current condition $U/r = U_0$, a certain outer current I is necessary, the desired flash current I_k being indicated by $I_k = I/c$. From Figs. 8 and 9 frontal short circuit (flash) current densities of 22·5 and 60 mA cm^{-2}, respectively, are derived. Only slightly higher values are familiar to the dry battery specialist: in D-size (IEC-R 20) dry cells for flashlight use, about 150 mA cm^{-2} values are found. Inserting, however, the large thickness $L = 15$ cm, the volumetric short circuit (flash) current density is evaluated as only 1·5 and 4 mA cm^{-3}, which is exceedingly low. Again comparing the D-size cell, one would expect 300 mA cm^{-3}, in industrial cells even much more.

7. Time dependent ionic resistivity

Under certain circumstances, the current distribution in a porous electrode can be influenced severely by inhomogeneous resistivities [27–30]. In porous electrodes having admixed electronic resistivity, e.g. graphite or carbon black, the electronic resistivity ρ_e remains fairly constant during the discharge. In spite of this, the ionic resistivity ρ_i rises considerably. The integral resistivity ρ of a flat porous electrode can be written simply

$$\rho \approx \frac{\rho_e \rho_i}{\rho_e + \rho_i} + (A\bar{\eta})/(LI),$$

where A is the geometric area and L is the thickness of the electrode, $\bar{\eta}$ its mean overvoltage and I the entire electrode current. By the application of alternating current, of frequency about 30 kHz, the faradaic electrode processes can be neglected, thus giving

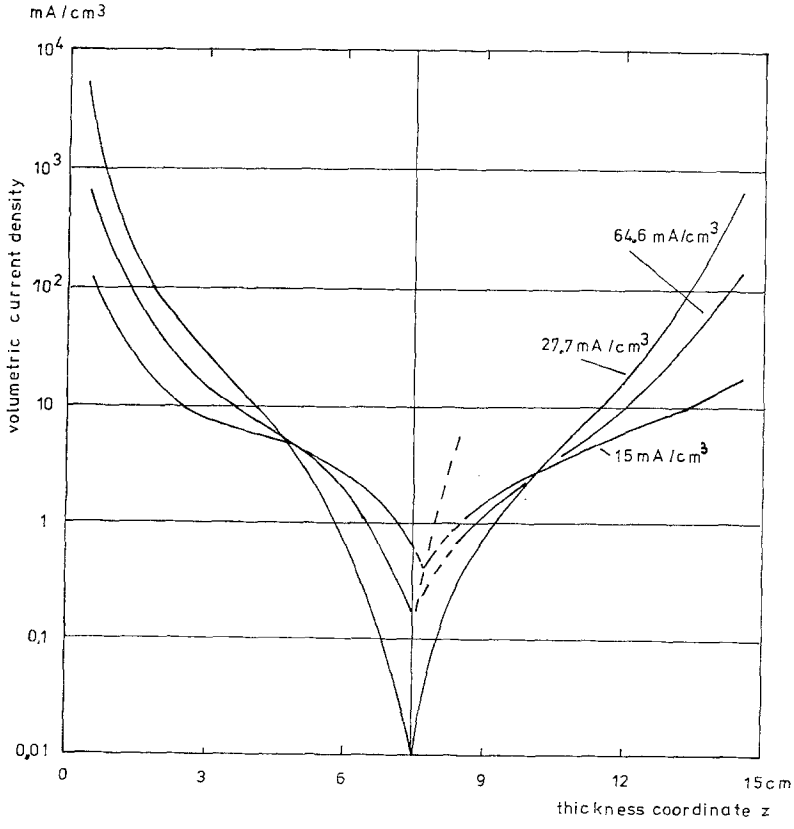

Fig. 9. Current distribution taken from a non-linear chain network representing a thick MnO_2 electrode having elevated electronic conductivity, parameters see Table 4, except electronic resistivity here $\rho_e = 2$ Ohm cm.

$$\rho \approx \frac{\rho_e \rho_i}{\rho_e + \rho_i}.$$

Assuming, as stated above that ρ_e remains constant, the development of ρ_i depending on time t or extracted electric charge $\int i\,dt$ in mA cm^{-3} can be followed. Again the measured functions have to be extrapolated to the electrode thickness $L \to 0$. Similarly as mentioned above with the overvoltage functions, interlayer diffusion is excluded also here. This may play a role for the inner electrode parts, but there the volumetric current density i is very low, and consequently the ionic resistivity changes only slowly.

Overvoltage functions are stable. Even the application of non-linear approximations seems justified. Resistivity changes during the discharge, however, are much less typical, and much less reproducible. Discharging and extrapolating to the thickness $L \to 0$ various electrodes having only small formula differences, at the 100 h rate, we observed a rise of the integral a.c. resistivity from 3·8 to 5·6 or even to 6·4 Ohm cm. Assuming $\rho_e = 7{\cdot}5$ Ohm cm remaining constant, the ionic resistivity ρ_i rises from about $\rho_i = 7{\cdot}7$ to 22 or even 44 Ohm cm. The rise proceeds in two steps: up to 100 mAh cm^{-3} electric charge being extracted, ρ_i remains nearly constant; later on this is followed by a steep increase. These figures can be given only with reserve, because the evaluating method as well as the reproducibility are unsatisfactory. This again evidences that current distributions cannot be predicted precisely, because the parameters are not sufficiently known [26]. Clearly, possible errors in ρ_i arise, as ρ_e becomes smaller. Thus, the following investigation will be restricted to the case of normal carbon black masses according to Table 4 and Fig. 8.

The rise of the ionic resistivity to, for example, triple the starting value in the most inner and outer layers can be introduced in the non-linear analogue just by enlarging the first and last R_i (compare Fig. 1). The consequence is a nearly twofold increase of the volumetric current density i in the last slice, $14 < z < 15$ cm, in Fig. 8. Between $0 < z < 2$ cm and $12 < z < 14$ cm the volumetric current density i drops markedly, compensating the increase at the right (electrolyte) border. The predicted short circuit (flash) current drops down from $i_k \approx 1{\cdot}5$ to below 0·7 mA cm^{-3}. Thus, we have to state, that the rising ionic resistivity renders the current distribution worse.

8. Discussion

The overvoltage of porous battery electrodes follows, as far as the electrode types investigated, linear, logarithmic or intermediate functions. These can be generated by electronic components. Practical electrodes are sufficiently stable and reproducible, to allow the necessary measurements, which have to be extrapolated to the electrode thickness zero. Inserting these functions of overvoltage which deviate from the linear approxi-

Table 4. Data of a 15 mesh non-linear network representing a MnO_2 electrode having a thickness of 150 mm

composition of the electrode mix:	80 pct. electrolytic manganese dioxide 10 pct. carbon black 10 pct. NH_4Cl
electrolyte composition: free, with gelling agents	70 pct. water 20 pct. NH_4Cl 10 pct. $ZnCl_2$
temperature:	20° C
dimensions:	thickness $L = 150$ mm, divided into 15 equal parts, each represented by one network mesh, 14 closed, one bisected at both ends area A = 1 cm^2 the choice of A is free and insignificant
electric parameters:	electronic resistivity $\rho_e = 7{\cdot}5$ Ohm cm ionic resistivity $\rho_i = 7{\cdot}5$ Ohm cm

overvoltage according to Fig. 4 assumed to be logarithmic, represented by 15 equal pn-diodes OA 20. Current degression factor $c = 0{\cdot}010$ cm^3, voltage surmount factor $r = 4{\cdot}0$, both together resulting in resistors R_e and R_i enlarged by a factor $w = r/c = 400$.

mation results in some practical cases in significant by changed current distributions. Landings or shoulders in the distribution curves occur with the non-linear analogues, which were not known so far. The treated example of a very thick MnO_2 electrode can be transferred easily to common electrodes having thicknesses of only a few milimetres. The shoulders will ameliorate the current distribution in both cases. Also the incorporation of better electronic conductors, compare Figs. 8 and 9, will have the same effect in thick as well as in thin electrodes.

The time or charge dependent ionic resistivity of the outer electrode layers, on the other hand, will not be observed as strongly marked in thin electrodes as here proposed for the thick electrode. In other words, in thin electrodes, the rise of ionic resistivity is much more uniform over the thickness. Nevertheless, rising ionic resistivity will, anyway, render the current distribution worse. Growing potential profiles inside the electrode are to be expected. Their treatment by corresponding networks or chain circuits will be investigated in a succeeding paper.

Acknowledgement

The measurements have partly been made ten years ago at Frankfurt in the research laboratory of the Varta Battery AG. The authors wish to thank Professor H. Bode and Professor G. Lander for their kind permission to use these results. The remainder of the measurements and calculations were made in the Laboratory of Practical Physics of the Gesamthochschule (Integral University) at Kassel. We are indebted to Mrs Ursula Stassinet for preparing several electric analogues, to Mr Robert Kirchhoff for measuring several resistivities, and to Mr Ulrich Euler for valuable help during the extended numerical treatment of the problem.

References

[1] P. Schoop, 'Handbuch der elektrischen Accumulatoren', Verlag Ferdinand Enke, Stuttgart, (1898).
[2] K.-J. Eulert, *Technik-Geschichte* **38** (1971) 339.
[3] K. Fischbeck and E. Einecke, *Z. anorg. Chem.* **148** (1925) 97.
[4] *Idem, ibid* **167** (1927) 21.
[5] *Idem, ibid* **175** (1928) 335.
[6] *Idem, ibid* **175** (1928) 341.
[7] V. S. Daniel'Bekh, *Zh.fiz. Khim. SSR* **22** (1948) 697.
[8] J. J. Coleman, *Trans. Electrochem. Soc.* **90** (1946) 545.
[9] *Idem, Zh. fiz. Khim. SSR* **29** (1953) 1323.
[10] *Idem, J. Electrochem. Soc.* **98** (1954) 26.
[11] K.-J. Euler, *Naturwiss.* **45** (1958) 537.
[12] *Idem, Physikal. Verhandl.* **9** (1958) 224.
[13] *Idem, Z. Electrochem.* **63** (1959) 537.
[14] *Idem, Z. angew. Physik* **29** (1970) 264.
[15] *Idem, Electrochim. Acta* **7** (1962) 205.
[16] *Idem, ibid* **13** (1968) 1533.
[17] K.-J. Euler, B. Seim and U. Euler, (in preparation).
[18] K.-J. Euler and W. Nonnenmacher, *Electrochim. Acta* **2** (1960) 268.
[19] K.-J. Euler, R. Ludwig and K.-N. Müller, *ibid* **9** (1964) 495.
[20] W. Stein, Thesis Aachen (1959).
[21] *Idem, Naturwiss.* **45** (1958) 459.
[22] J. S. Newman and C. W. Tobias, *J. Electrochem. Soc.* **109** (1962) 1183.
[23] E. A. Grens II, Ph.D. Thesis University of California, at Berkely (1963).
[24] R. N. Fleck, D. N. Hanson, C. W. Tobias, *AEC C Contract No. W-7405-eng-48,* University of California at Berkeley.
[25] R. C. Alkire, Ph.D. Thesis, University of California and Berkeley (1968).
[26] K.-J. Euler and K.-J. Müller, *Electrochim. Acta* **8** (1963) 849.
[27] K.-J. Euler, *Naturwiss.* **56** (1969) 326.
[28] K.-J. Euler, *Electrochim. Acta* **15** (1970) 1233.
[29] K.-J. Euler, *Chem.-Ing.-Tech.* **43** (1971) 1310.
[30] U. Erdmann and K.-J. Euler, *Elektrotech. Z.* **A95** (1974) 339.